# A Photometric Study of the Near-Contact Binary CE Pegasi

**Edward J. Michaels**
*Waffelow Creek Observatory, 10780 FM 1878, Nacogdoches, TX 75961; astroed@ejmj.net*

*Received April 21, 2026; revised May 6, 2026; accepted May 7, 2026*

**Abstract** Presented are multi-band photometry for the eclipsing binary CE Pegasi observed on 17 nights in August and September 2025. A photometric light curve solution was derived from the Wilson-Devinny program using observations from five passbands (B, V, g', r', and i'). The results indicate that CE Peg is a semidetached near-contact binary with a mass ratio of q = 0.315 and an orbital inclination of 83°. The cooler K6 secondary star fills its Roche lobe and the F0 primary nearly so with a filling factor of 96.8%. The period analysis using 35 minima timings, spanning 30 years, found an unchanging orbital period of 0.6420292 d.

## 1. Introduction

The variability of CE Peg (2MASS J21404695+2509153, HV 6156, NSVS 8776019, GSC 02193-01640) was discovered by Shapley and Hughes (1940) while searching for variable stars at high galactic latitudes. They classified this star as an eclipsing binary with an orbital period of 0.6420 day and a visual magnitude range of 13.2–14.2. Several more recent low cadence surveys have also identified its eclipsing binary light variations: The All-Sky Automated Survey, the Northern Sky Variability Survey, and the All-Sky Automated Survey for Supernovae (ASAS; Pojmański 2002; NSVS, Woźniak *et al.* 2004; ASAS-SN, Jayasinghe *et al.* 2018). Using the NSVS database Hoffman *et al.* (2008) classified CE Peg as a β Lyrae eclipsing binary. The light curves of β Lyrae stars display unequal primary and secondary minima and are continuously changing in brightness between eclipses due to ellipsoidal variations. Their evolutionary states range from two detached main sequence stars in tight orbits, to semidetached binaries with mass transfer, to near-contact binaries (NCB) with a highly evolved secondary and less evolved primary. Detailed photometric analysis and period studies of β Lyrae systems can provide valuable insight into understanding the physical characteristics of these binaries.

In this paper high cadence multi-band photometric observations of CE Peg are presented in section 2. An orbital period analysis and updated ephemerides are presented in section 3. Photometric solutions using the 2015 version of the Wilson-Devinny (WD) program are presented in section 4. Discussion of the results is presented in section 5 and conclusions in section 6.

## 2. Photometric observations

Photometric observations were acquired in August and September 2025 using the Waffelow Creek Observatory's 0.36-m Ritchey-Chrétien telescope (https://obs.ejmj.net; see the Table 1 Observation Log). The telescope was equipped with a Johnson-Sloan multicolor QHY268M camera that gives a 29' × 19' field-of-view. VOYAGER software was used for automated image acquisition and DONUTS for improved photometric precision (Voyager 2024; McCormac 2013). DONUTS is an autoguiding algorithm that fixes the stars on the same sensor pixels for each image acquired throughout the observing campaign. Observations were taken in five passbands, Johnson B and V, and Sloan g', r', and i'. The light images were calibrated using bias, dark, and flat frames. MIRA software was used for image calibration and differential aperture photometry (Mirametrics 2024). The Figure 1 chart shows the locations of the comparison and check stars and Table 2 lists their coordinates, and standard magnitudes from the AAVSO Photometric All-Sky Survey database (APASS; Henden *et al.* 2015). The instrumental magnitudes of each observation were converted to standard magnitudes and the Heliocentric Julian Date (HJD) to orbital phase (φ). Figure 2 shows the observed light curves with orbital phase plotted from –0.6 to 0.6 with negative phase defined as (φ–1). The light curve properties for each passband are listed in Table 3. The check star magnitudes were plotted each night with no significant variability detected (see bottom panel of Figure 2). The check star standard deviations ranged from 3 to 5 mmag. The flatness of the secondary minimum indicates a total eclipse with an approximate duration of 34 minutes. All the observations can be accessed through the AAVSO International Database (Kafka 2017).

## 3. Period analysis and ephemerides

A literature search located 31 minima timings for this star with an additional 4 timings determined from the new observations using the Kwee and van Woerden (1956) method. An initial linear ephemeris was formed from the earliest primary minima timing available and the orbital period taken from the AAVSO Variable Star Index (VSX; Watson *et al.* 2014):

$$\text{HJD Min I} = 2450030.372\ (3) + 0.64202\ \text{E}. \quad (1)$$

The timings and their errors (if available) are collected in Table 4. Included in this table are the cycle numbers and the difference between the observed and the predicted minima times (O–C) calculated from Equation 1. An updated linear ephemeris was computed by least-squares:

$$\text{HJD Min I} = 2460923.6816\ (2) + 0.6420291(9)\ \text{E}. \quad (2)$$

This ephemeris was used to phase the observations. Figure 3 shows the residuals from Equation 1 (top panel) and the best-fit linear line of Equation 2. The residuals from the Equation 2 fit

are shown in the bottom panel of Figure 3. The residuals give little indication of a secular or a cyclic period change in the 30 years covered by the minima timings.

## 4. Light curve analysis

### 4.1. Color, temperature, spectral type, absolute magnitude, and luminosity

The photometric observations for each color were binned in both phase and magnitude using a phase width of 0.01. The observations falling into each bin were averaged in both phase and magnitude. The resulting 100 normal points for each color were used for light curve modeling. The binned Johnson B and V magnitudes were linearly interpolated to form (B–V) color indices. The mean observed color over the full phase range is (B–V) = 0.564 ± 0.006. The color excess, obtained from dust maps based on Pan-STARRS1 and 2MASS photometry and Gaia parallaxes, was used to correct for interstellar reddening (Green *et al.* 2018). The color excess is $E(B–V) = 0.040 \pm 0.006$. To correct for extinction in the V passband, the extinction-to-reddening ratio of $A_V / E(B–V)$ gives a value of $A_V = 0.123 \pm 0.018$.

The LAMOST Low-Resolution Spectroscopic Survey (DR11) obtained a spectrum of CE Peg on November 13, 2020 (Figure 4). The LAMOST pipeline found an effective temperature and spectral type, $T_{eff} = 7063 \pm 100$ K and F0. This is in good agreement with a value derived from Gaia DR3 data, $T_{eff} = 7079 \pm 97$ K (2024 SHBoost Catalog: Khalatyan *et al.* 2024). The LAMOST value was assigned to the primary star for light curve modeling.

The absolute visual magnitude, $M_V = 2.51 \pm 0.01$, was determined from the mean-apparent magnitude corrected for extinction, $m_V = 12.77 \pm 0.02$, and the Gaia DR3 distance for this star, $d = 1107 \pm 14$ pc (Gaia Collaboration *et al.* 2023). Combining the computed absolute magnitude with the Sun's absolute magnitude gives a visual luminosity of $L_{V\odot} = 8.0 \pm 0.2$.

### 4.2. Synthetic light curve modeling

The light curves of CE Peg are best described as β Lyrae type. The continuous light variation indicates that the component stars are tidally distorted and the large difference in minima depths suggests a significant temperature difference between the component stars. These light curve properties suggest a semidetached or detached Roche configuration with the stars nearly in contact.

For modeling, the 100 normal points for each light curve were converted to flux with an average of 6 observations per normal point (see section 4.1). BINARY MAKER 3.0 software was used to make the preliminary fits to each light curve (BM3; Bradstreet and Steelman 2002). The stellar and orbital parameters from each BM3 fit were averaged. These parameters were used as the starting inputs for the computation of simultaneous five-color light curve solutions using the WD program (Wilson and Devinney 1971; van Hamme and Wilson 1998). The following WD settings were used for solution iterations:

- Each normal point was assigned a weight equal to the number of observations forming that point
- Radiative treatment—Kurucz model stellar atmospheres
- Effective temperature of primary star fixed at $T_1 = 7063$ K
- Logarithmic limb-darkening coefficients calculated using the method of van Hamme (1993)
- The WD program was set to Mode-2 for detached binaries
- Standard radiative parameters were assigned to the primary star and convective parameters for the secondary star:
  gravity brightening: $g_1 = 1.0$, $g_2 = 0.32$ (von Zeipel 1924; Lucy 1968)
  bolometric albedo: $A_1 = 1.0$, $A_2 = 0.5$ (Ruciński 1969)
- Adjustable parameters: inclination (i), mass ratio ($q = M_2 / M_1$), potentials ($\Omega_1$, $\Omega_2$), temperature of the secondary star ($T_2$), band-specific luminosity for each wavelength (L), and third light ($L_3$).

The parameter subscripts 1 and 2 refer to the hotter and cooler component stars, respectively.

For the first WD solution attempt, convective parameters were assigned to both stars. The solution iterations did converge, but the resulting synthetic light curves fit the observed secondary eclipse poorly and both stars exceeded their critical lobes. The primary star's effective temperature is in the region where energy transport in the outer envelope of main sequence stars transitions from convective to radiative. A second attempt using standard radiative parameters for the primary star resulted in a much-improved fit. The solution parameters are shown in column 2 of Table 5. This solution indicates CE Peg is semidetached with the secondary star filling its Roche lobe.

The observed light curves are reasonably symmetric with Max I and Max II nearly the same brightness (see Table 3). The fit between the observed and synthetic light curves was very good except for a small deficit of light between secondary minimum and Max II (see Figure 5). This asymmetry is apparent in each color. This may indicate the presence of a cool spot(s) on the facing hemisphere of the secondary star. Cool spots are not unexpected, given this star's rapid rotation and convective envelope. The BM3 program was used to model this small asymmetry by placing a cool spot on the secondary star. The spot parameters, latitude, longitude, spot size, and temperature factor were adjusted until a good fit was obtained. The best-fit parameters were then incorporated into a new WD model. The final WD solution parameters are shown in column 3 of Table 5. The comparison of the parameter values between the two solutions shows they are essentially the same, except for a 63% reduction in residuals for the spotted model. The top panel of Figure 6 displays the spotted model fits overlaid onto the observed light curves and the middle panel the residuals. The bottom panel shows the WD model color curves overlaid onto the observed (B–V) curves. A graphical presentation of the CE Peg system is shown in Figure 7 (Bradstreet and Steelman 2002). The third-light corrections ($L_3$) were negligibly small or negative throughout the solution process. The solution mass ratio, q = 0.3154, should be well determined, given the total secondary eclipse (Wilson 1978; Terrell and Wilson 2005).

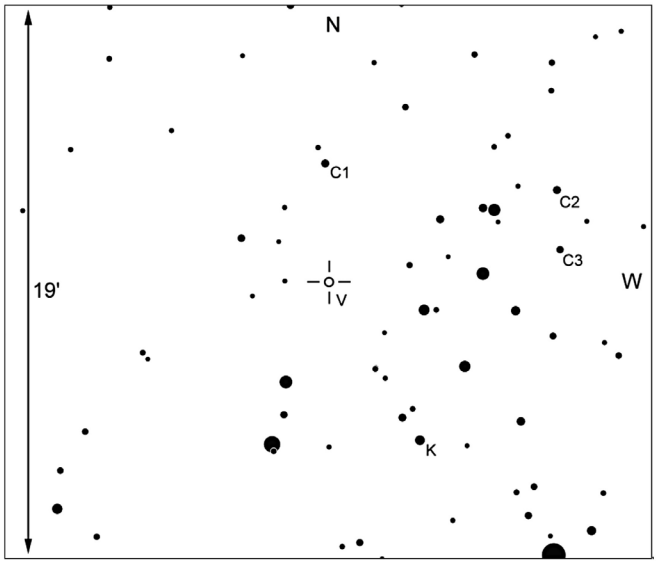


Figure 1. Finder chart for CE Peg (V), comparison (C), and check (K) stars. This chart was generated by the AAVSO Variable Star Plotter (Craig *et al.* 2023).

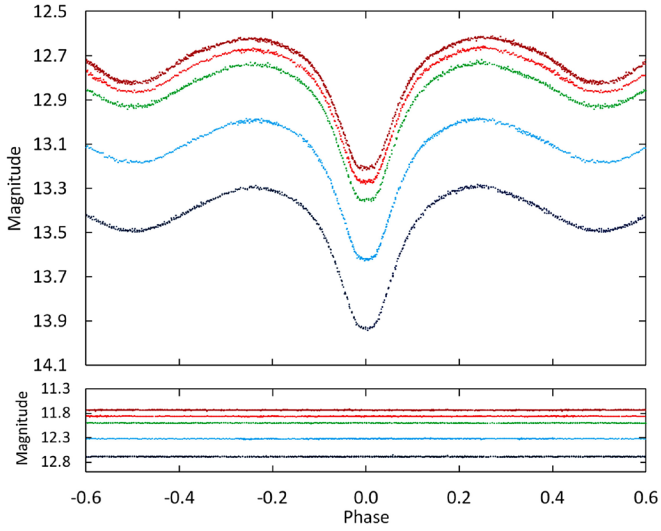


Figure 2. The folded CCD light curves in standard magnitudes. From top to bottom the passbands are i', r', V, g', and B. In the same order, the bottom curves are the check-star magnitudes. Error bars were omitted from the plotted points for clarity.

Table 1. Observation log.

| *Filter* | *Dates (2025)* | *No. Nights* | *No. Images* |
|---|---|---|---|
| B | Aug 24, 25; Sep 2, 3, 4, 10 | 6 | 571 |
| V | Aug 24, 25; Sep 2, 3, 4, 10 | 6 | 573 |
| g' | Aug 15, 16, 17, 19 | 4 | 505 |
| r' | Aug 15, 16, 17, 19 | 4 | 511 |
| i' | Sep 11, 12, 15, 16, 23, 25, 26 | 7 | 900 |

Table 2. Standard comparison and check star magnitudes.

| *System* | *R.A. (2000)* *h* | *Dec. (2000)* ° | *B* | *V* | *g′* | *r′* | *i′* |
|---|---|---|---|---|---|---|---|
| CE Peg | 21.67971 | +25.15422 | -- | -- | -- | -- | -- |
| GSC 02193-01747 (C) | 21.67987 | +25.22196 | 13.302 | 12.639 | 12.944 | 12.514 | 12.403 |
| GSC 02193-00681 (C) | 21.67005 | +25.20674 | 13.438 | 12.686 | 13.054 | 12.540 | 12.393 |
| GSC 02193-01692 (C) | 21.66993 | +25.17271 | 13.722 | 12.981 | 13.317 | 12.819 | 12.679 |
| GSC 02193-01763 (K) | 21.67586 | +25.06409 | 12.664 | 11.996 | 12.311 | 11.862 | 11.747 |
| *Mean magnitudes of the K-star observations* | | | 12.686 ± 0.004 | 11.991 ± 0.003 | 12.314 ± 0.005 | 11.855 ± 0.004 | 11.727 ±0.004 |

Table 3. Average light curve properties.

| | *Min I Mag.* | *Min II Mag.* | *Δ Mag. Min II – Min I* | *Max I Mag.* | *Max II Mag.* | *Δ Mag. Max II – Max I* | *Mag. Range Max I – Min I* |
|---|---|---|---|---|---|---|---|
| B | 13.933 ±0.006 | 13.489 ±0.006 | –0.444 ±0.009 | 13.291 ±0.004 | 13.297 ±0.006 | 0.006 ±0.007 | 0.639 ±0.008 |
| V | 13.350 ±0.004 | 12.928 ±0.006 | –0.422 ±0.007 | 12.730 ±0.007 | 12.740 ±0.006 | 0.009 ±0.009 | 0.611 ±0.008 |
| g' | 13.621 ±0.004 | 13.178 ±0.002 | –0.442 ±0.005 | 12.989 ±0.005 | 12.994 ±0.007 | –0.005 ±0.009 | 0.627 ±0.008 |
| r' | 13.270 ±0.005 | 12.861 ±0.005 | –0.410 ±0.011 | 12.660 ±0.003 | 12.673 ±0.002 | 0.013 ±0.011 | 0.597 ±0.011 |
| i' | 13.208 ±0.005 | 12.822 ±0.006 | –0.386 ±0.007 | 12.616 ±0.003 | 12.623 ±0.003 | 0.007 ±0.004 | 0.586 ±0.005 |

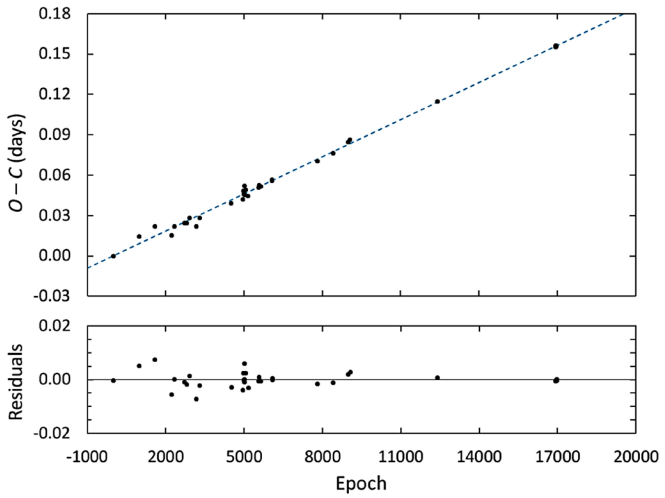


Figure 3. The top panel shows the O–C residuals calculated from the linear ephemeris of Equation 1 (filled circles). The dashed line is the linear best-fit from Equation 2. The bottom panel shows the residuals from the linear fit.

Table 4. Times of minima and O–C residuals.

| *Type* | *Epoch HJD 2400000+* | *Error* | *Cycle No.* | *(O–C)* | *Reference* |
|---|---|---|---|---|---|
| ccd | 50030.3720 | 0.0031 | 0.0 | 0.00000 | 1 |
| ccd | 50660.5290 | 0.0056 | 981.5 | 0.01437 | 1 |
| ccd | 51043.5017 | 0.0005 | 1578.0 | 0.02214 | 2 |
| ccd | 51465.3019 | 0.0030 | 2235.0 | 0.01520 | 3 |
| ccd | 51535.2888 | 0.0063 | 2344.0 | 0.02192 | 3 |
| ccd | 51780.5428 | 0.0029 | 2726.0 | 0.02428 | 4 |
| ccd | 51838.3247 | 0.0030 | 2816.0 | 0.02437 | 4 |
| ccd | 51899.3205 | 0.0030 | 2911.0 | 0.02824 | 4 |
| ccd | 52062.3874 | 0.0067 | 3165.0 | 0.02210 | 5 |
| ccd | 52144.5722 | 0.0013 | 3293.0 | 0.02834 | 6 |
| ccd | 52929.4523 | — | 4515.5 | 0.03899 | 7 |
| ccd | 53216.4383 | 0.0022 | 4962.5 | 0.04205 | 8 |
| ccd | 53222.5437 | 0.0023 | 4972.0 | 0.04826 | 8 |
| ccd | 53233.4556 | 0.0013 | 4989.0 | 0.04582 | 8 |
| ccd | 53242.4442 | 0.0011 | 5003.0 | 0.04614 | 8 |
| ccd | 53250.4697 | 0.0022 | 5015.5 | 0.04639 | 8 |
| ccd | 53251.4318 | 0.0027 | 5017.0 | 0.04546 | 8 |
| ccd | 53257.5378 | 0.0007 | 5026.5 | 0.05227 | 8 |
| ccd | 53284.4996 | 0.0007 | 5068.5 | 0.04923 | 8 |
| ccd | 53341.3138 | 0.0008 | 5157.0 | 0.04466 | 9 |
| ccd | 53599.4120 | — | 5559.0 | 0.05082 | 10 |
| ccd | 53613.5379 | 0.0007 | 5581.0 | 0.05228 | 11 |
| ccd | 53613.5381 | 0.0006 | 5581.0 | 0.05248 | 12 |
| ccd | 53651.4164 | 0.0006 | 5640.0 | 0.05160 | 11 |
| ccd | 53936.4777 | 0.0006 | 6084.0 | 0.05602 | 13 |
| ccd | 53936.4783 | 0.0003 | 6084.0 | 0.05662 | 14 |
| ccd | 55048.4709 | 0.0003 | 7816.0 | 0.07058 | 15 |
| ccd | 55428.5524 | 0.0022 | 8408.0 | 0.07624 | 16 |
| ccd | 55806.3898 | 0.0026 | 8996.5 | 0.08487 | 17 |
| ccd | 55849.7277 | 0.0004 | 9064.0 | 0.08642 | 18 |
| ccd | 57993.4609 | 0.0023 | 12403.0 | 0.11484 | 19 |
| ccd | 60903.7781 | 0.0001 | 16936.0 | 0.15536 | 20 |
| ccd | 60912.7670 | 0.0002 | 16950.0 | 0.15598 | 20 |
| ccd | 60921.7555 | 0.0002 | 16964.0 | 0.15620 | 20 |
| ccd | 60923.6811 | 0.0002 | 16967.0 | 0.15577 | 20 |

*References: (1) Šafář and Zejda (2000a); (2) Šafář and Zejda (2000b); (3) Šafář and Zejda (2002); (4) Luboš (2007); (5) Zejda (2004); (6) Diethelm (2001); (7) Hübscher (2005); (8) Hübscher* et al. *(2005); (9) Diethelm (2005); (10) Le Borgne and Klotz (2006); (11) Hübscher* et al. *(2006); (12) Zejda (2006); (13) Hübscher and Walter (2007); (14) Hübscher (2007); (15) Hübscher* et al. *(2010); (16) Hübscher (2011); (17) Hübscher and Lehmann (2012); (18) Diethelm (2012); (19) Pagel (2021); (20) this paper.*

Table 5. Results derived from WD light curve modeling.

| *Parameter* | *No Spot* | *Spot* |
|---|---|---|
| i (°) | 83.1 ± 0.2 | 83.1 ± 0.2 |
| $T_1$ (K) | [1]7063 | [1]7063 |
| $T_2$ (K) | 4346 ± 14 | 4346 ± 10 |
| $\Omega_1$ | 2.569 ± 0.002 | 2.569 ± 0.001 |
| $\Omega_2$ | 2.500 ± 0.007 | 2.500 ± 0.005 |
| q ($M_2/M_1$) | 0.3154 ± 0.0008 | 0.3154 ± 0.0006 |
| $L_1/(L_1+L_2)$ (B) | 0.987 ± 0.011 | 0.987 ± 0.008 |
| $L_1/(L_1+L_2)$ (V) | 0.972 ± 0.011 | 0.972 ± 0.008 |
| $L_1/(L_1+L_2)$ (g') | 0.982 ± 0.011 | 0.982 ± 0.008 |
| $L_1/(L_1+L_2)$ (r') | 0.960 ± 0.012 | 0.960 ± 0.008 |
| $L_1/(L_1+L_2)$ (i') | 0.944 ± 0.012 | 0.944 ± 0.009 |
| $r_1$ side | 0.4686 ± 0.0004 | 0.4706 ± 0.0004 |
| $r_2$ side | 0.2765 ± 0.0013 | 0.2873 ± 0.0013 |
| filling factor$_1$ | 96.8% | 96.8% |
| filling factor$_2$ | 99.7% | 99.7% |
| *Cool spot* | | *Star 2* |
| colatitude (°) | — | 66 ± 4 |
| longitude (°) | — | 347 ± 1 |
| spot radius (°) | — | 30 ± 4 |
| temp. factor | — | 0.85 ± 0.04 |
| Residuals | 0.00060 | 0.00038 |

*Note: The errors in the stellar parameters result from the least-squares fit to the model. The actual uncertainties are considerably larger. The subscripts 1 and 2 refer to the star being eclipsed at primary and secondary minimum respectively.*
*[1] Parameters not adjusted.*

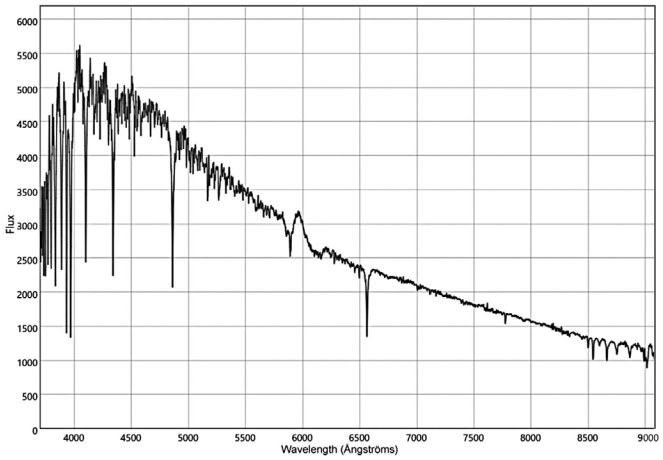


Figure 4. LAMOST low resolution spectrum of CE Peg.

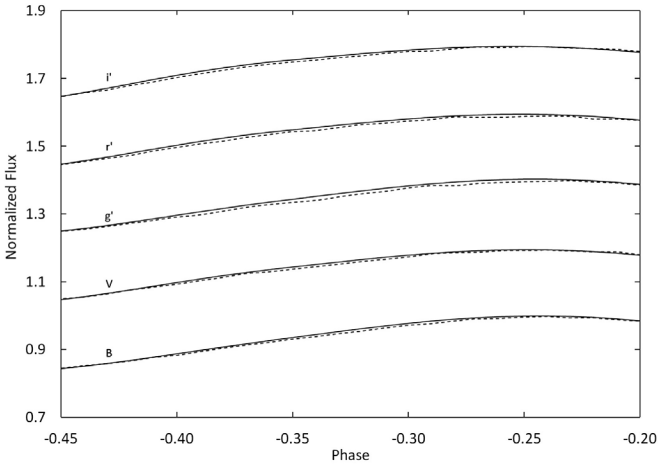


Figure 5. Enlarged view of observed light curves (dashed line) and the WD spotless model light curves (solid line). The deficit of light between orbital phase –0.45 and –0.25 indicates a possible cool spot on the secondary star.

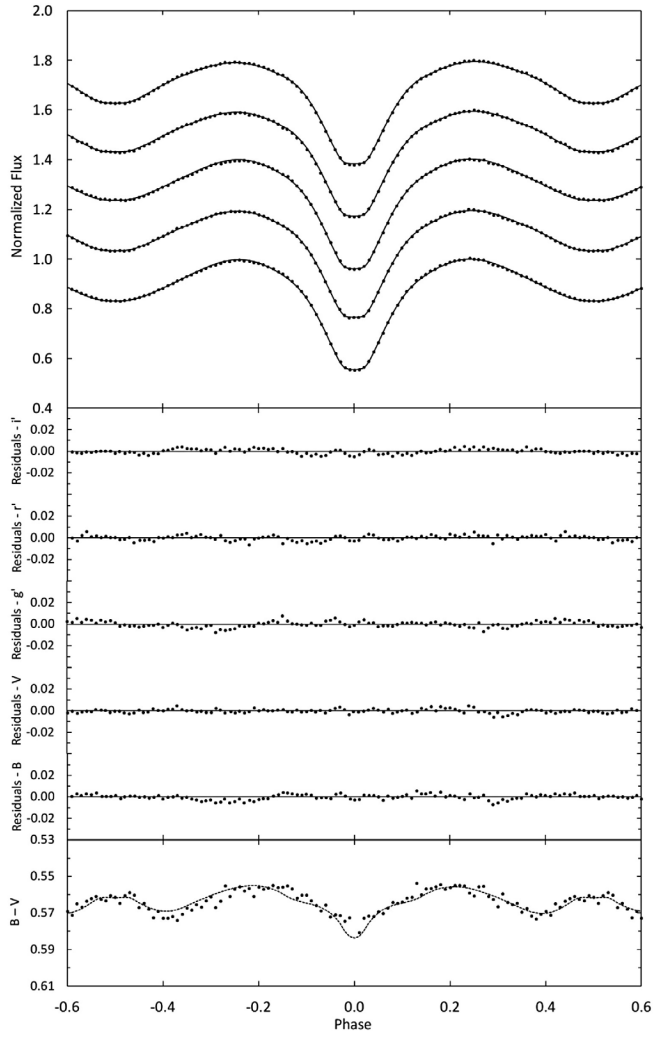


Figure 6. The top panel shows a comparison between the WD best-fit model (solid curves) and the observed normalized flux curves. From top to bottom, the passbands are i', r', g', V, and B with each light curve offset by 0.2. The residuals are shown in the middle panel. The bottom panel displays the (B–V) color curves. The observed colors are the filled circles, and the dashed line is the color variations calculated from the WD model. Error bars are omitted from the plotted points for clarity.

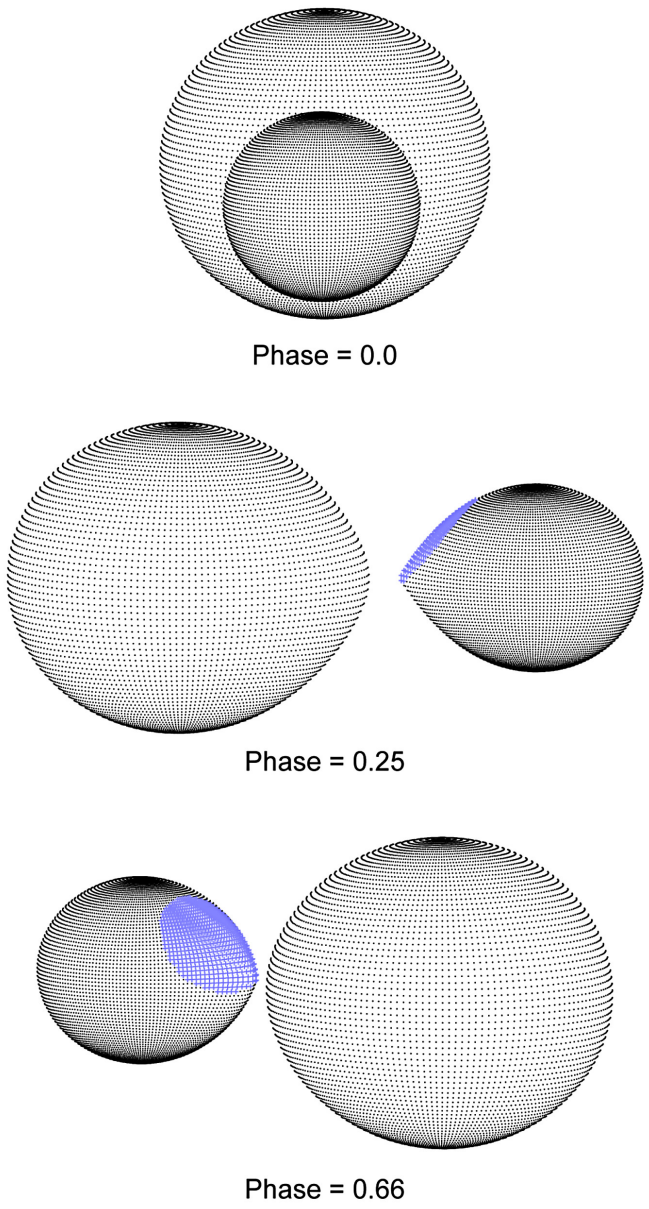


Figure 7. Roche lobe surfaces for the best-fit WD model.

As an additional check, a q-search was performed by completing several WD solutions using a set of fixed mass ratios that ranged from 0.29 to 0.35. The results show a well-defined minimum near 0.32, which is in good agreement with the solution mass ratio (see Figure 8).

## 5. Discussion

CE Peg has the characteristics of a near-contact binary (NCB) which include strong tidal interactions, facing surfaces that are less than 0.1 radii apart, and orbital periods that are less than one day (Shaw 1990). The WD light curve solution gives a semidetached SD2 Roche configuration due to the cooler, less massive secondary star filling its critical surface (Shaw 1994; Yakut and Eggleton 2005). The hot primary star almost fills its Roche lobe with a filling-factor of 96.8% (see Figure 9). Other properties of SD2 type binaries include symmetrical light curves

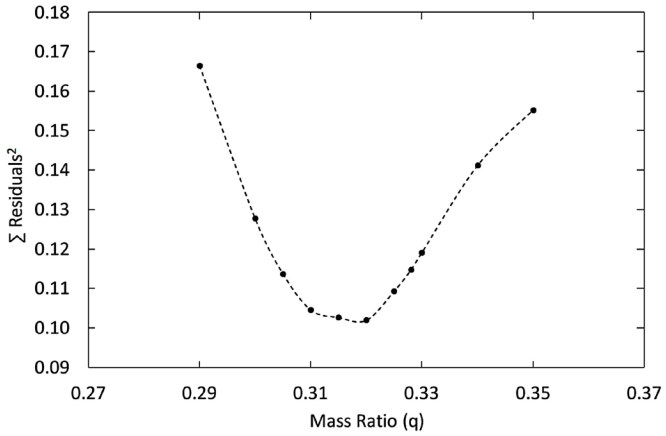


Figure 8. The q-search results show the relation between the sum of the residuals squared and the mass ratio.

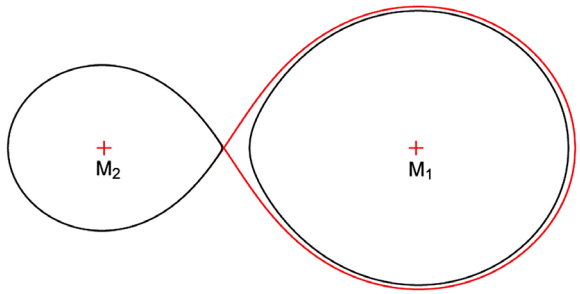


Figure 9. Roche configuration in the orbital plane. The red line denotes the critical lobe and the black lines the potential surfaces of the two stars for the WD solution. The mass center of each star is labeled.

(no O'Connell effect) and orbital periods that are increasing due to conservative mass transfer from the less massive to the more massive star. The observed light curves are symmetrical with Max I equal to Max II, but the period study (section 3) showed an orbital period that is constant. This inconsistency may be the result of a combination of angular momentum loss from magnetic braking, which works to shorten the orbital period, and the rate of mass transfer, which would lengthen the period. These two mechanisms may be strongly competitive in semidetached systems (Nanouris *et al.* 2011, 2015; Erdem and Öztürk, 2014).

The absolute stellar parameters of the component stars can be estimated using the WD solution mass ratio and an approximate mass of the primary star. For short period Algol and NCB binaries, the primary component is likely to be an unevolved main sequence star (Shaw 1994; Yakut and Eggleton 2005; Stępień and Kiraga 2013). The mass of the primary star was interpolated from the online table of Pecaut and Mamajek (2013) using its effective temperature. The secondary star mass was calculated by combining the primary star mass and the mass ratio. The distance between the mass centers of the component stars was found using Newton's form of Kepler's Third Law (Equation 3),

$$P^2 = \frac{4\pi^2 a^3}{G(M_1 + M_2)}. \quad (3)$$

The bolometric magnitudes, radii, and surface gravities of each star were taken from the output of the WD Light Curve program. Shaw (1994) found the radii of SD2 secondary stars are 2 to 3 times larger compared to main sequence stars of the same mass. The radius of CE Peg's secondary star is oversized by a factor of 2.3. The stellar luminosities were calculated by combining the bolometric magnitudes of the stars and the sun. The provisional stellar parameter values have been collected in Table 6.

Table 6. Provisional absolute parameters.

| *Parameter* | *Symbol* | *Value* |
|---|---|---|
| Stellar masses | $M_1$ ($M_\odot$) | 1.52 ± 0.06 |
| | $M_2$ ($M_\odot$) | 0.48 ± 0.02 |
| Semimajor axis | a ($R_\odot$) | 3.95 ± 0.06 |
| Mean stellar radii | $R_1$ ($R_\odot$) | 1.84 ± 0.03 |
| | $R_2$ ($R_\odot$) | 1.12 ± 0.02 |
| Bolometric magnitude | $M_{bol,1}$ | 2.54 ± 0.06 |
| | $M_{bol,2}$ | 5.72 ± 0.15 |
| Stellar luminosity | $L_1$ ($L_\odot$) | 7.57 ± 0.42 |
| | $L_2$ ($L_\odot$) | 0.40 ± 0.06 |
| Surface gravity | log $g_1$ (cgs) | 4.09 ± 0.03 |
| | log $g_2$ (cgs) | 4.02 ± 0.03 |

*Note: The calculated values in this table are provisional. Radial velocity observations are necessary for direct determination of $M_1$, $M_2$, and a.*

The visual luminosities of the component stars, $L_{1V}$ = 8.1 ± 0.5 and $L_{2V}$ = 0.22 ± 0.03, were computed using the bolometric corrections taken from the online tables of Pecaut and Mamajek (2013). Summing gives a system luminosity of $L_V$ = 8.3 ± 0.5 $L_\odot$, which is in good agreement with the value determined from observed quantities, $L_V$ = 8.0 ± 0.2 $L_\odot$ (see section 4.1). The distance to this binary, d = 1128 ± 35 pc, was derived from the system visual luminosity and the extinction corrected apparent magnitude. This value is consistent with the distance from Gaia astrometry, d = 1107 ± 14 pc.

## 6. Conclusions

The new high cadence multiband observations of CE Pegasi revealed β Lyrae type light curves. The hotter primary star occults the smaller star, causing a brief total eclipse at secondary minimum. The photometric solution was derived based on the B, V, g', r', and i' observations. CE Peg is a near-contact SD2-type binary with the secondary star filling its Roche lobe and the primary star nearly filling its lobe (98.6%). The system has a mass ratio of q = 0.315 and an orbital inclination of 83.1°. The spectral types of the main sequence primary and the oversized secondary stars are F0 and K6, respectively. The small light curve asymmetries were addressed by modeling a single cool spot on the facing hemisphere of the secondary star. The ephemeris was updated using new minima timings from the observations. The period analysis gave little indication of a secular period change over the past 30 years.

## 7. Acknowledgements

This research was made possible using the AAVSO Photometric All-Sky Survey (APASS), funded by the Robert Martin Ayers Sciences Fund. This research has made use of the SIMBAD database and the VizieR catalog access tool, operated

at CDS, Strasbourg, France. This study made use of data acquired by the Large Sky Area Multi-Object Fiber Spectroscopic Telescope (LAMOST). This is a national scientific research facility operated by the National Astronomical Observatories, Chinese Academy of Sciences. This work has made use of data from the European Space Agency (ESA) mission Gaia (https://www.cosmos.esa.int/gaia), processed by the Gaia Data Processing and Analysis Consortium (DPAC, https://www.cosmos.esa.int/web/gaia/dpac/consortium). Funding for the DPAC has been provided by national institutions, particularly the institutions participating in the Gaia Multilateral Agreement.

**References**

Bradstreet, D. H., and Steelman, D. P. 2002, *Bull. Amer. Astron. Soc.*, **34**, 1224.

Craig, M., Beck, S., Otero, S., and Pablo, B. 2023, AAVSO Variable Star Plotter (https://apps.aavso.org/vsp).

Diethelm, R. 2001, *BBSAG Bull.*, No. 126, 1 (http://www.variables.ch/images/BBSAG/B126.pdf).

Diethelm, R. 2005, *Inf. Bull. Var. Stars*, No. 5653, 1.

Diethelm, R. 2012, *Inf. Bull. Var. Stars*, No. 6011, 1.

Erdem, A., and Öztürk, O. 2014, *Mon. Not. Roy. Astron. Soc.*, **441**, 1166.

Gaia Collaboration, *et al.* 2023, *Astron. Astrophys.*, **674A**, 1.

Green, G. M., *et al.* 2018, *Mon. Not. Roy. Astron. Soc.*, **478**, 651.

Henden, A. A., *et al.* 2015, AAVSO Photometric All-Sky Survey, data release 9. (https://www.aavso.org/apass).

Hoffman, D., Harrison, T. E., Coughlin, J. L., McNamara, B. J., Holtzman, J. A., Taylor, G. E., and Vestrand, W. T. 2008, *Astron. J.*, **136**, 1067.

Hübscher, J. 2005, *Inf. Bull. Var. Stars*, No. 5643, 1.

Hübscher, J. 2007, *Inf. Bull. Var. Stars*, No. 5802, 1.

Hübscher, J., and Lehmann, P. B. 2012, *Inf. Bull. Var. Stars*, No. 6026, 1.

Hübscher, J., Lehmann, P. B., Monninger, G., Steinbach, H.-M., and Walter, F. 2010, *Inf. Bull. Var. Stars*, No. 5941, 1.

Hübscher, J, Paschke, A., and Walter, F. 2005, *Inf. Bull. Var. Stars*, No. 5657, 1.

Hübscher, J., Paschke, A., and Walter, F. 2006, *Inf. Bull. Var. Stars*, No. 5731, 1.

Hübscher, J. 2011, *Inf. Bull. Var. Stars*, No. 5984, 1.

Hübscher, J., and Walter, F. 2007, *Inf. Bull. Var. Stars*, No. 5761, 1.

Jayasinghe, T., *et al.* 2018, *Mon. Not. Roy. Astron. Soc.*, **477**, 3145.

Kafka, S. 2017, Variable star observations from the AAVSO International Database, (https://www.aavso.org/aavso-international-database).

Khalatyan, A., *et al.* 2024, *Astron. Astrophys.*, **691A**, 98.

Kwee, K. K., and van Woerden, H. 1956, *Bull. Astron. Inst. Netherlands*, **12**, 327.

Le Borgne, J.-F., and Klotz, A. 2006, *GEOS Notes Circ.*, **1039**, 1.[1]

Luboš, B. *et al.* 2007, *Open Eur. J. Var. Stars*, **74**, 1.

Lucy, L. B. 1968, *Astrophys. J.*, **151**, 1123.

McCormac, J., Pollacco, D., Skillen, I., Faedi, F., Todd, I., and Watson, C. A. 2013, *Publ. Astron. Soc. Pacific*, **125**, 548.

Mirametrics. 2024, Image Processing, Visualization, Data Analysis (https://www.mirametrics.com).

Nanouris, N., Kalimeris, A., Antonopoulou, E., and Rovithis-Livaniou, H. 2011, *Astron. Astrophys.*, **535A**, 126.

Nanouris, N., Kalimeris, A., Antonopoulou, E., and Rovithis-Livaniou, H. 2015, *Astron. Astrophys.*, **575A**, 64.

Pagel, L. 2021, *BAV J.*, No. 52, 1. (http://bav-astro.de).

Pecaut, M., and Mamajek, E. E. 2013, *Astrophys. J., Suppl. Ser.*, **208**, 9.[2]

Pojmański, G. 2002, *Acta Astron.*, **52**, 397.

Ruciński, S. M. 1969, *Acta Astron.*, **19**, 245.

Šafář J., and Zejda, M. 2000a, *Inf. Bull. Var. Stars*, No. 4887, 1.

Šafář J., and Zejda, M. 2000b, *Inf. Bull. Var. Stars*, No. 4888, 1.

Šafář J., and Zejda, M. 2002, *Inf. Bull. Var. Stars*, No. 5263, 1.

Shapley, H. and Hughes, E. M. 1940, *Ann. Astron. Obs. Harvard Coll.*, **90**, No. 4, 163.

Shaw, J. S. 1990, in: *Proceedings of the NATO Advanced Study Institute on Active Close Binaries*, ed. C. Ibanoglu, Kluwer, Dordrecht, 241.

Shaw, J. S. 1994, *Mem. Soc. Astron. Ital.*, **65**, 95.

Stępień, K., and Kiraga, M. 2013, *Acta Astron.*, **63**, 239.

Terrell, D., and Wilson, R. E. 2005, *Astrophys. Space Sci.*, **296**, 221.

van Hamme, W. 1993, *Astron. J.*, **106**, 2096.

van Hamme, W. and Wilson, R. E. 1998, *Bull. Amer. Astron. Soc.*, **30**, 1402.

von Zeipel, H. 1924, *Mon. Not. Roy. Astron. Soc.*, **84**, 702.

Voyager. 2024, Systems Integration Software (https://software.starkeeper.it/).

Watson, C., Henden, A. A., and Price, A. 2014, AAVSO International Variable Star Index VSX (Watson+, 2006–2014 (https://www.aavso.org/vsx).

Wilson, R. E. 1978, *Astrophys. J.*, **224**, 885.

Wilson, R. E., and Devinney, E. 1971, *Astrophys. J.*, **166**, 605.

Woźniak, P., *et al.* 2004, *Astron. J.*, **127**, 2436.

Yakut, K., and Eggleton, P. P. 2005, *Astrophys. J.*, **629**, 1055.

Zejda, M. 2004, *Inf. Bull. Var. Stars*, No. 5583, 1.

Zejda, M., Mikulasek, Z., and Wolf, M. 2006, *Inf. Bull. Var. Stars*, No. 5741, 1.

[1] Le Borgne and Klotz (2006): https://rr-lyr.irap.omp.eu/documents/GEOS_circulars/NC1039.pdf

[2] Pecaut and Mamajek (2013): http://www.pas.rochester.edu/~emamajek/EEM_dwarf_UBVIJHK_colors_Teff.txt